Effects of Reynolds number on some properties of a turbulent jet from a long square pipe

M. Xu, A. Pollard, J. Mi, F. Secretain, and H. Sadeghi

Citation: Physics of Fluids (1994-present) **25**, 035102 (2013); doi: 10.1063/1.4797456
View online: http://dx.doi.org/10.1063/1.4797456
View Table of Contents: http://scitation.aip.org/content/aip/journal/pof2/25/3?ver=pdfcov
Published by the AIP Publishing

PHYSICS OF FLUIDS **25**, 035102 (2013)

Effects of Reynolds number on some properties of a turbulent jet from a long square pipe

M. Xu,[1,2,3] A. Pollard,[1,a)] J. Mi,[2,a)] F. Secretain,[1] and H. Sadeghi[1]
[1]*Department of Mechanical and Materials Engineering, Queen's University at Kingston, Ontario K7L 3N6, Canada*
[2]*State Key Laboratory of Turbulence and Complex Systems, College of Engineering, Peking University, Beijing 100871, China*
[3]*Marine Engineering College, Dalian Maritime University, Dalian 116026, China*

(Received 14 November 2012; accepted 4 March 2013; published online 28 March 2013)

The flow in the near-to-intermediate field of a jet emanating from a long square pipe is investigated using hot-wire anemometry. The data include distributions of the mean and high order turbulence moments over $8000 < \mathrm{Re} < 50\,000$ along the jet centreline. It is demonstrated that the far-field rates of the mean velocity decay and spread, as well as the asymptotic value of the streamwise turbulent intensity, all decrease as Re increases for $\mathrm{Re} \leq 30\,000$; however, they become approximately Re-independent for $\mathrm{Re} > 30\,000$. It follows that the critical Reynolds number should occur at $\mathrm{Re_{cr}} = 30\,000$. Attention is given to the exponents associated with the compensated axial velocity spectra that show that the inertial subrange calculated according to isotropic, homogeneous turbulence emerges at $x/D_e = 30$ for all Re; however, if the scaling exponent is altered from $\mathrm{m} = -5/3$ to between $-1.56 < \mathrm{m} < -1.31$ the "inertial" range emerges at lower values of Re and the exponent is Re dependent. It is also found that the exponent agrees very well with Mydlarski and Warhaft correlation $m = (5/3)(1-3.15\mathrm{R}_\lambda^{-2/3})$, where R_λ is the Taylor Reynolds number, obtained for turbulence decay behind a grid. © *2013 American Institute of Physics*. [http://dx.doi.org/10.1063/1.4797456]

I. INTRODUCTION

The study of turbulent jets has become a common topic in turbulence. There are a number of studies that have explored the effects of Reynolds number on the spatial evolution of the mean and higher order statistics of jets that issue from round and non-round nozzles or orifices.

Recently, Fellouah *et al.*[1] and Fellouah and Pollard[2] investigated the effect of Reynolds number on the near- and intermediate-field regions of a round nozzle jet using flying and stationary hot-wire measurements. They considered the velocity spectra and turbulence length scale distributions in the range of $6000 \leq \mathrm{Re_h} \leq 100\,000$ and explored the idea of mixing transition as proposed by Dimotakis.[3] They found that the mixing transition is highly spatial and Re dependent. They also identified mixing transition through the emergence of an inertial subrange based upon compensated axial velocity spectra.

It is well known that inlet conditions affect higher order statistics in a round jet, see, for example, Hussain,[4] George,[5] Xu and Antonia,[6] Uddin and Pollard.[7] A recent review paper may also be consulted, Ball *et al.*[8]

From another perspective, the exit geometry of the jet flow has also been found to have an important influence on the behavior of jet flow. Noncircular jets have been found more effective to mix with ambient fluid than comparable circular jets, and thus they have been investigated extensively in the literature.[9–25] In the case of square jets in particular, it is known from large eddy

[a)]Authors to whom correspondence should be addressed. Electronic addresses: pollard@me.queensu.ca and jcmi@coe.pku.edu.cn.

simulation (LES) at laboratory scale Reynolds numbers that the vortex structure plays a significant role in the enhanced mixing associated with these jets relative to unforced round jets, see Grinstein and DeVore[26] and Grinstein *et al.*[11] The reason(s) for the enhanced mixing include the initial vortex structures downstream near the exit of the square jet, which through simple Biot-Savart arguments give rise to collapse of the vortex in the corner regions and eventual axis switching; there are other spatial events that occur that present longitudinally oriented vortex structures, see Gutmark and Grinstein,[12] which in the case of round jets (called braids) have been shown to increase entrainment and by inference the mixing, see Liepmann and Gharib,[27] Citriniti and George,[28] and McIlwain and Pollard.[29]

The flow under consideration is no different to any jet flow: they are equally complex in flow structure in the near-to-intermediate field, whether the jet is round, square or other shape. What is fundamentally different between the current square jet arrangement and a round jet that issues from a contraction nozzle is the lack of a true potential core in the former. In a round jet, the potential core preserves the turbulence level and distribution derived from its upstream conditioning, which, based upon the literature, is invariably presumed to be fine-scaled. However, there is enough literature that demonstrates that both within the shear layers and beyond the potential core the turbulence is highly three-dimensional irrespective of the initial condition.

In the case of square jets, there appears to be no data for flow emanating from a long square tube, the flow inside of it gives rise to weak cross stream secondary flows induced by anisotropy of the Reynolds stresses. Grinstein *et al.*[11] considered a square pipe jet with a length to diameter ratio of about 4.5, so it is unlikely that their flow was fully developed at the jet exit. It is hypothesized here that the secondary flows should alter the evolution of the jet, as they would instill an additional instability mechanism. That is, the inlet conditions would change with Reynolds number since it is known that the strength of the secondary flow is Reynolds number dependent, see Pinelli *et al.*[30] as well as Brundrett and Baines.[31] This also recognizes that jets are sensitive to inlet conditions, see, for example, George[5] and Uddin and Pollard.[7] At the Reynolds numbers considered in this paper, Kajishima and Miyake,[32] used large eddy simulation of square duct flow at $\mathrm{Re} = 6200$ and 67 400. They compared their predictions to experimental data available at that time for $\mathrm{Re} = 42\,000$ obtained by Melling and Whitelaw,[33] 83 000 by Brundrett and Baines,[31] 215 000 by Launder and Ying,[34] and 250 000 by Gessner and Emery.[35] At $\mathrm{Re} \sim 65\,000$, they found agreement between experiment and simulations of a variety of turbulence quantities along the duct wall bisector to be reasonable in the core region, but less so as the corner was approached. Grinstein *et al.*[11] considered the cases of $\mathrm{Re} = 9300$ and 42 000 but did not present data for cross-stream turbulence quantities. It is clear that a jet that emanates from a long square duct will have imprinted on it a complex three-dimensional flow structure that is probably more complicated than just the near wall turbulence structures formed on the inside surface of a round jet contraction nozzle. Therefore, the reader of the current paper must be cognizant of these differences.

In this paper, data are presented that in the first instance characterizes the mean and Reynolds stress distribution in the near to intermediate field of a square jet that emanates from a long square duct with sharp corners over $8000 < \mathrm{Re} < 50\,000$. These data are further processed to highlight changes in the compensated axial velocity spectra to show that the inertial subrange calculated according to isotropic, homogeneous turbulence emerges at a $\mathrm{Re} = 20\,000$; however, if the spectra scaling exponent is altered from a $-5/3$ to approximately $-3/2$, as suggested by Mi and Antonia,[36] the "inertial" range emerges at lower values of Re. The implications of this on the mixing transition are discussed.

The rest of the paper is arranged as below. Section II provides experimental details. In Sec. III, the experimental results are presented and discussed. Finally, conclusions are provided in Sec. IV.

II. EXPERIMENTAL DETAILS

The present square jets were generated from a nozzle system whose schematic diagram is shown in Fig. 1(a). Air was generated by a fan, which was mounted on anti-vibration pads, powered by an electric motor and controlled by a variable frequency drive. Then, the airflow to the square jet was initially conditioned in a settling chamber equipped with three air filters, a flow straightener, and

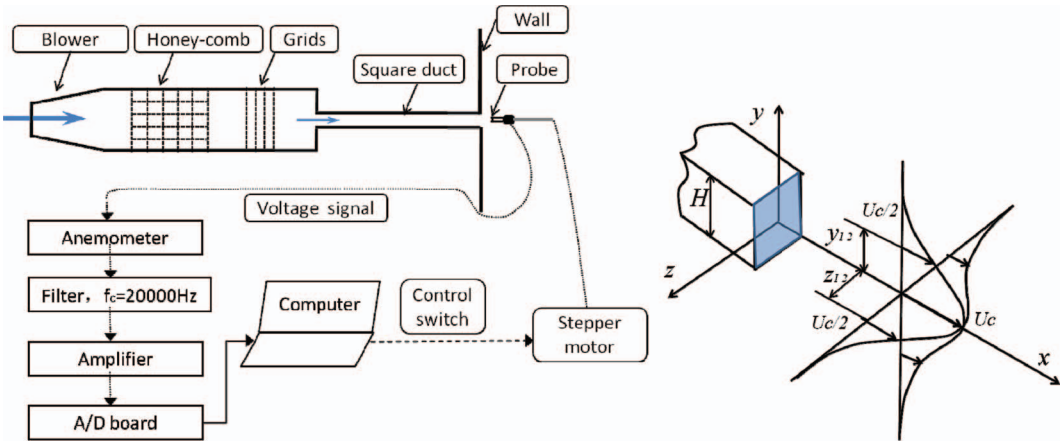

FIG. 1. Schematic of the experimental arrangement (left) and three-dimensional square jet nozzle exit, jet notation and coordinate system (right).

a wire mesh. The purpose of the settling chamber was to break up any large-scale structures and reduce the overall turbulence intensity.

There are mainly three different types of square jet nozzles used in the literature: contractions, orifice plates, and long ducts. In the case of long ducts, the lowest bulk Re considered here is higher than the most recent direct numerical simulations.[30] To enable future simulations to proceed, the present facility consisted of a square duct that was 2.5 cm^2 and approximately 2 m in length. The nominal opening area $A = 6.25$ cm^2 and the equivalent diameter D_e [$\equiv 2(A/\pi)^{1/2}$] was approximately 2.82 cm. The exit of the square duct was installed at the centre of an impermeable Perspex® wall of 3 m $\times$ 3 m. Thus, the entrainment into the jet occurred only from the lateral and spanwise directions. The apparatus was situated in a large room. However, irrespective of the size of the room, entrainment and jet development (boundary) conditions were restricted to axial locations where the effect of confined spaces were deemed small; this was confirmed by ensuring that at the highest Re numbers, mean axial centreline velocity decayed as x^{-1}, where x is the downstream distance measured from the nozzle exit (see Fig. 1(b)). The mean streamwise velocity U_j at the centre of the square exit plane was varied over the range $4.2 \leq U_j \leq 26.4$ m/s, which corresponds to a Reynolds number range $8 \times 10^3 < \mathrm{Re} < 5 \times 10^4$, where $\mathrm{Re} \equiv U_j D_e/\nu$.

The measurements were taken between $0 \leq x/D_e \leq 40$ using a single hot-wire anemometer under isothermal conditions of ambient temperature 22.0 °C $\pm$ 0.1 °C. An Auspex single hot-wire sensor was used (tungsten wire of diameter $d_w = 5$ μm and length $l_w = 1$ mm), with an overheat ratio of 1.5. To avoid aerodynamic interference of the prongs on the hot-wire sensor, the present probe was carefully mounted with prongs parallel to the square jet axis.

Due to the complex near-field flow field, the reader should be cautioned that the present results maybe influenced by the limitations from the use of a single hot-wire. However, it is worth noting that Mi and Antonia[37] performed measurements of the mean and RMS velocities, as well as those of their lateral gradients, using single and one or four X-wire probes, in the turbulent wake of a circular cylinder. These authors demonstrated that the single hot-wire probe measured reasonably well in the wake flow at $x/d = 20$ (here d is the cylinder diameter), obtaining nearly identical results as from the X-wire probe (see their Figs. 2 and 5). The flow under present consideration is no more highly three-dimensional than the wake flow. Accordingly, we are confident that the present single hot-wire measurements should not result in statistics that would lead to wrong conclusions.

Calibrations of the hot-wire were conducted using a standard Pitot static tube connected to a digital pressure transducer (Datametrics model 590D) prior to and after each set of measurements. For each U_j or Re_d, different ranges of velocity were used in the calibration from 0.5 $\sim$ 3 m/s to 0.5 $\sim$ 30 m/s. The calibration data were fit using a 3rd order polynomial. Both calibration functions were checked for discrepancies, and the experiments were repeated

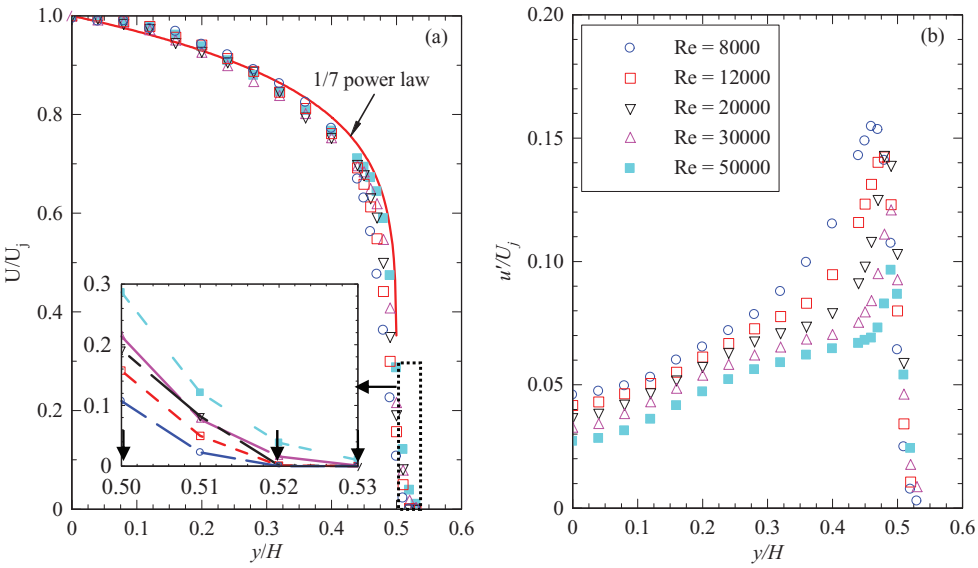

FIG. 2. Inflow conditions at $x/D_e = 0.05$ for different Reynolds numbers. (a) Normalized mean velocity; (b) turbulence intensity. Note that the inset panel indicates location (Y) used for integral calculations (see Eqs. (4) and (5)).

if the velocity drift exceeded 0.5%. The average accuracy of each calibration was found to be within ±0.2%.

Velocity signals were low pass filtered with an identical cut-off frequency of $f_c = 20$ kHz for all measurements to eliminate excessively high-frequency noise and to avoid aliasing. To obtain the maximum possible signal-to-noise ratio, the mean voltages were sampled and removed from the signals by means of the offset and the remaining fluctuations were amplified by a factor of 20 before they were sampled. The voltage signals were then digitized on a personal computer at $f_s = 40$ kHz via a 12 bit A/D converter and each record had a duration of about 80 s. In addition, control of the hot-wire position and data acquisition was accomplished using the National Instruments software LABVIEW, as indicated in Fig. 1(a).

To remove the effect of high frequency noise, the present data were filtered using the digital scheme of filtering high-frequency noise used by Mi *et al.*[38,39] This iterative scheme obtains "true" values of the Kolmogorov time scale η and frequency f_K by filtering the measured velocity signal u_m, where the subscript m means "measured," based on Eqs. (1)–(3) below. Suppose that the measured dissipation rate ε_m can be expressed as

$$\varepsilon_m = \varepsilon[\text{true dissipation}] + \varepsilon_n[\text{noise contribution}] = \gamma\varepsilon \tag{1}$$

and $\gamma = (1 + \varepsilon_n/\varepsilon) > 1$. Substituting (1) into the definition of the Kolmogorov scale, i.e., $\eta \equiv (\nu^3/\varepsilon)^{1/4}$, leads to

$$\eta_m = [\nu^3/(\gamma\varepsilon)]^{1/4} = \gamma^{-1/4}\eta, \tag{2}$$

thus,

$$f_{Km} = \gamma^{1/4} f_K, \tag{3}$$

where $f_K \equiv U/(2\pi\eta)$ and U is the streamwise mean velocity.

The scheme uses (1)–(3) iteratively to "squeeze out" the noise contribution from u_m by filtering u_m at new f_{Km}. The principle is based on the fact that the noise imposes a significantly greater influence on ε_m than on both η_m and f_{Km}. For instance, when $\varepsilon_m = 5\varepsilon$, the resulting values of η_m and f_{Km} are $\eta_m = 0.67\eta$ and $f_{Km} = 1.5\,f_K$.

The direct measurement of ε requires measurements of all 12 gradients in ε (see, e.g., Ref. 40), which are not realizable in the current experiments. Accurate measurement of any component of ε requires a multi-sensor probe with exceptionally high spatial and temporal resolution to resolve

the finest-scale or most-rapid fluctuations of velocity. In this context, the present study estimates ε from hot-wire measurements of $u(t)$, using the isotropic relation $\varepsilon = 15\nu\ \langle(\partial u/\partial x)^2\rangle$ together with Taylor's hypothesis $\langle(\partial u/\partial x)^2\rangle = U^{-2}\langle(\partial u/\partial t)^2\rangle$. Here, $u(t)$ was substituted for $u_1(t)$, which is the streamwise velocity component.

III. PRESENTATION AND DISCUSSION OF RESULTS

A. Inlet conditions

To quantify the exit conditions of the jet, the mean and RMS velocities (U, $u' = \langle u^2\rangle^{1/2}$) were measured for each Re at $x/D_e = 0.05$ in the spanwise direction over the range $0 \le y/H \le 0.55$, where H is the width of the square duct. Spanwise profiles of U/U_j and u'/U_j are presented in Figs. 2(a) and 2(b), respectively. In all cases, approximate power law mean exit velocity profiles were obtained. As Re was increased from 8000 to 50 000, the dependence of the mean axial velocity exit profile on Re is not obvious. A plot of the mean velocity profile at Re = 8000 and 50 000 (see Fig. 2(a), inset) shows that the mean velocity profile of Re = 50 000 is higher than that of any other Re in the region of $0.5 < y/H < 0.55$. In addition, the mean velocity profile tends to follow a 1/7th power law profile with increased Re. However, there is a strong Re dependence of the exit flow on the distribution and magnitude of the turbulence intensity, Fig. 2(b). The central portion and the peak value of u'/U_j in the shear layer both decrease with Re. In the central portion, u'/U_j decreases from 0.045 to 0.027, and the peak value of u'/U_j reduces from 0.155 to 0.09. This trend coincides with the finding of Deo *et al.*[41] for a plane jet. The change in the initial velocity profiles due to the Re variation are expected to cause different downstream development of the flow features in each jet flow. For example, Kajishima and Miyake[32] reported marked changes in the distribution of the mean streamwise and secondary flow intensity along the square duct bisector using LES at Re = 6200 and Re = 67 400; while these early LES results are not conclusive, they do suggest that the current results may be influenced in the very near field by these changes in initial conditions.

Here, the displacement thicknesses (δ) and momentum thickness (θ) of the boundary layer are calculated approximately from the mean velocity profiles and the momentum integral equations, viz.,

$$\delta = \int_0^{\mathrm{Y}} (1 - U/U_j)_{x=0.05D_e} dy, \tag{4}$$

$$\theta = \int_0^{\mathrm{Y}} U/U_j(1 - U/U_j)_{x=0.05D_e} dy. \tag{5}$$

Here, Y is the integral upper limit. Figure 3 presents the above parameters calculated from the profiles using "best-fit" spline curves and numerically integrating Eqs. (4) and (5) with different integral upper limit. Their normalizations are made by 0.5 H, which shows the relative magnitude of these thicknesses with respect to the pipe size. As shown in Fig. 3, δ obviously increases as the integral upper limit increases from 0.5 H to 0.53 H. However, the upper limit has little effect on θ, which converges for $Y \ge 0.52\,H$. In addition, it is interesting to note that δ decreases as Re increases, while θ approaches its maximum value at Re = 3×10^4. This is different to that of a plane jet, where both δ and θ monotonically decrease as Re increases before tending toward a constant value for Re > 10^4 (approximately).[41] Note there is no uniform region in the exit mean velocity profile of a square jet. The mean velocity decreases as the distance from the centreline increases. As shown in Fig. 2(a), the mean velocity profile is higher in the region of $0.4 < y/D_e < 0.5$, as well as lower in the region of $0.2 < y/D_e < 0.4$ for higher Reynolds number. This causes θ to not monotonically decrease as Re increases. Figure 3 also indicates small variation in the magnitudes of δ and θ for different Reynolds numbers, which suggests that the mean exit velocity has weak dependence on Reynolds number.

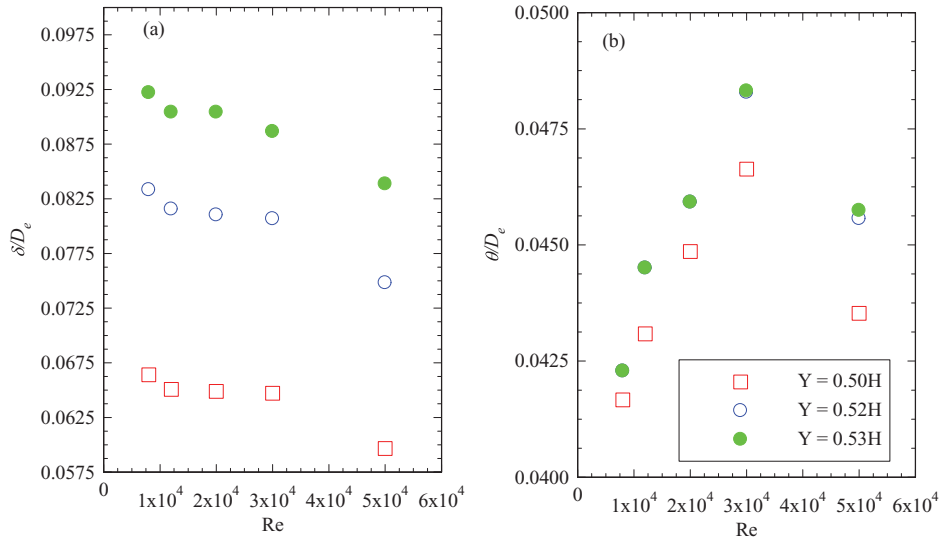

FIG. 3. Dependences of (a) displacement thicknesses (δ) and (b) momentum thickness (θ) on Reynolds number and integral upper limit (Y), Figure 2 and Eqs. (4) and (5).

B. The mean velocity field

Figure 4 presents the streamwise variation of the inverse centreline mean velocity U_c normalized by the exit velocity U_j, i.e., U_j/U_c for $8000 \leq \mathrm{Re} \leq 50\,000$. In the initial region, $x/D_e < 5$ (note that the use of the term "potential core" is not used here given the secondary flows emanating from the square duct), no significant Re_d-dependent variation in U_c is detected. However, farther downstream, the centreline mean velocity decays approximately inversely and linearly with axial distance. The decay rate of the mean velocity depends significantly on Re. The influence of Re on the flow sufficiently downstream maybe quantified using

$$U_c/U_j = K_U[(x - x_U)/d]^{-1}. \tag{6}$$

Here, the constant K_U is the slope of the linear curve of U_j/U_c, and x_U is the x-location of the virtual origin of (6). This relation becomes valid beyond $x/D_e > 16$; this location decreases with increasing Re. Significantly, the present data for different Reynolds numbers appear to converge asymptotically onto a single curve at $\mathrm{Re}_d \geq 3 \times 10^4$. Figure 5 demonstrates that the Re dependence of U_c embodied

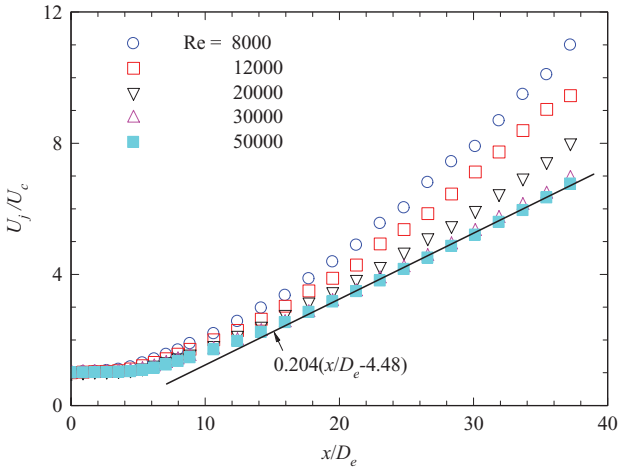

FIG. 4. Streamwise variations of U_j/U_c for $\mathrm{Re} = 8000 \sim 50\,000$.

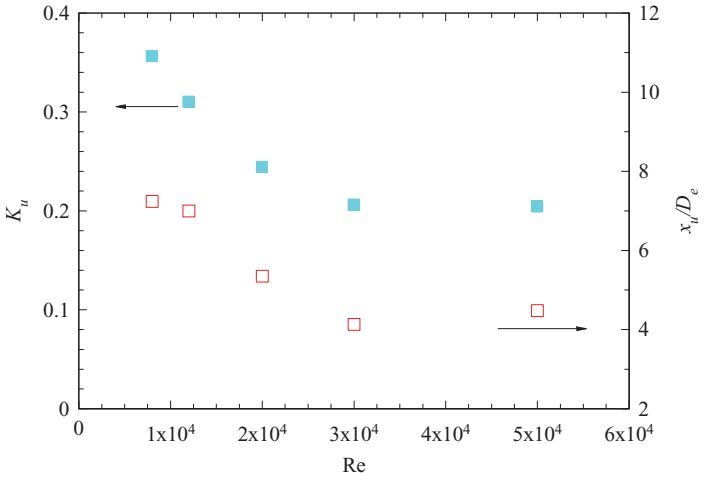

FIG. 5. Dependence on Re of K_U (open symbol) and x_U/D_e (closed symbol).

in K_U is significant for $\mathrm{Re} \leq 3 \times 10^4$ but weakens with further increase of Re. It follows that there appears to be a critical Reynolds number of $\mathrm{Re}_{cr} = 30\,000$ above which the asymptotic far-field value of K_U will be independent of Re. The dependence of x_U on Re follows a similar trend to that of K_U.

The lateral profiles of U/U_c at selected downstream locations for $\mathrm{Re}_d = 8000$–$50\,000$ are presented in Fig. 6. Here, the y-coordinate is normalized using the velocity half-width $Y_{1/2}$ where the mean velocity is half the centreline mean velocity, i.e., $0.5U_c$. As expected, the velocity profiles become self-similar closer to the nozzle exit as the Reynolds number increases. For instance, self-similarity appears to be attained at $x/D_e > 10$ for $\mathrm{Re} = 5 \times 10^4$ and at $x/D_e > 20$ for $\mathrm{Re} = 8 \times 10^3$. The self-similar velocity profiles conform closely to a Gaussian distribution $U/U_c = e^{-(y/Y_{1/2})\ln 2}$.

The influence of Re on the mean spread rate of the square jet is assessed from the downstream variation of the half-width $Y_{1/2}$. The magnitude of $Y_{1/2}$ reflects the overall rate of the spread. Figure 7 indicates that the half-widths vary linearly with x for $x/D_e > 10$ for all Reynolds numbers. This linear variation may be represented by

$$Y_{1/2}/D_e = K_Y[(x - x_Y)/D_e], \tag{7}$$

where K_Y reflects the jet-spread rate and x_Y is the x-location of the virtual origin. Figure 8 demonstrates that as Reynolds number increases from 8000 to 50 000, K_Y decreases asymptotically from about 0.11 to 0.08, which is consistent with that of K_U (Fig. 5). Taking them together, it is concluded that an increase in Re leads to reduced entrainment of the jet in the far field. This agrees with Deo *et al.*[41] for a plane jet. However, for the present square jet flow, the variation of $Y_{1/2}$ does not exhibit a local peak in the very near field region, the appearance of which is normally associated as evidence of axis-switching phenomenon for square jets.[42,43] Grinstein *et al.*[11] found no evidence of axis switching for jets emanating from their short-pipe square jet. Thus, the axis-switching is not likely to occur in the present square jet that issues from a long pipe. The main difference between the present jet flow and others investigated previously[11,43] is the nozzle type. For those jets from contracting nozzles or orifice plates, the momentum boundary thickness at the exit plane is much thinner than that from the long square duct. The thinner the momentum boundary thickness, the easier it seems to produce large vortex rings.[11] In the present jets, no obvious large vortex ring is produced because of the non-uniform velocity profile at the exit plane (see Fig. 2(a)) and the thick boundary layers.

Another significant point can be made from the data presented in Fig. 8. That is, similar to the centreline velocity decay rate, the critical Reynolds number for the asymptotic far-field spreading rate appears to occur at $\mathrm{Re}_{cr} = 30\,000$ above which the far-field spreading rate does not vary with

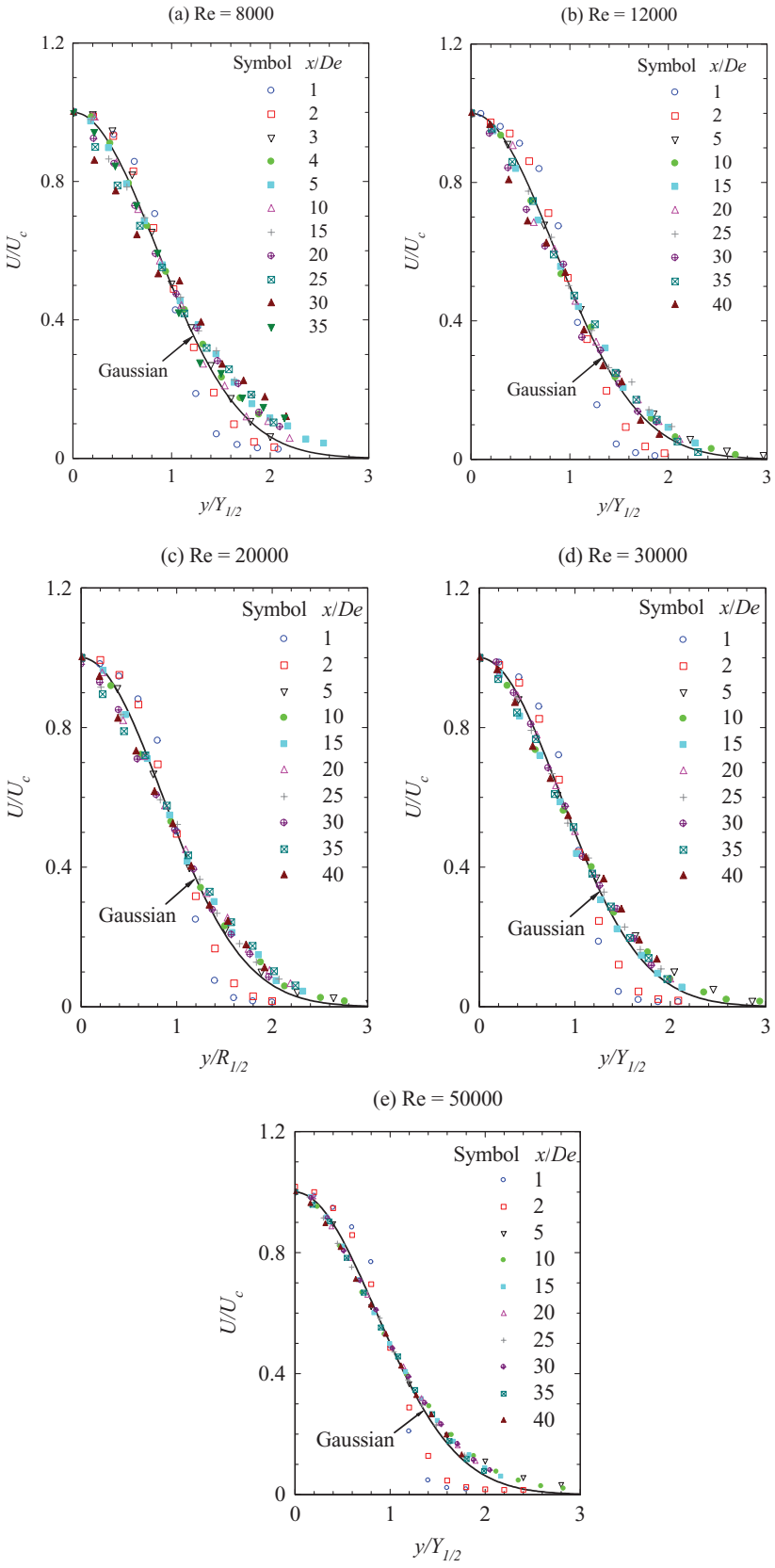

FIG. 6. Lateral distributions of U/U_c for Re = 8000–50 000.

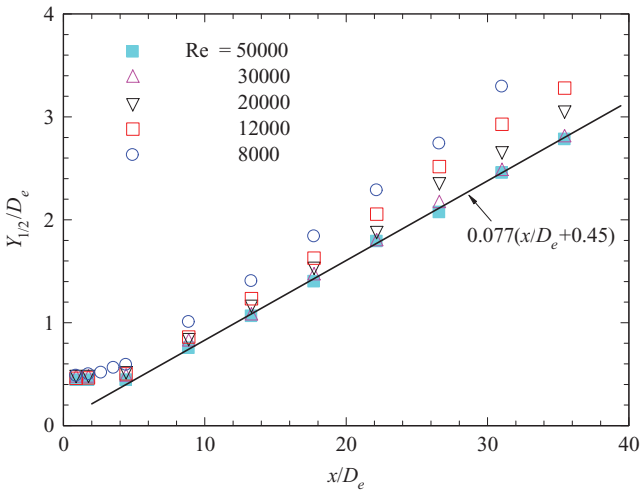

FIG. 7. Streamwise variations of $R_{1/2}/D_e$ for Re = 8000 ~ 50 000.

Re. Correspondingly, as Re increases, the x-location of the virtual origin of the jet half-width (x_Y) first decreases and before increasing beyond $\mathrm{Re}_{cr} = 30\,000$.

C. The fluctuating velocity field

Figure 9 presents data for the centreline evolution of the turbulence intensity (u'/U_c) at different Reynolds numbers. Evidently, u'/U_c grows rapidly in the initial region, which is caused by high local shear in the streamwise mean velocity. With increased distance from the exit, u'/U_c increases gradually and appears to asymptote to a constant value (K_u) in the far field (that is, beyond $x/D_e = 40$). However, the magnitudes of u'/U_c are Re dependent so that based on the averaged value of u'/U_c over the region $30 \le x/D_e \le 40$, the far-field K_u is seen to first decrease with Re and then asymptote to $K_u \approx 0.25$ for $Re_d \ge 30\,000$, see Fig. 10. Quinn and Militzer[43] data are also added in Fig. 11 for their case of Re = 184 000. Obviously, the asymptotic value of K_u for the present case of Re = 50 000 tends to be larger than that of Quinn and Militzer.[43] This is expected since their Re is much higher and K_u should decrease with Re (Fig. 10). Also of note, as will be presented next, the centreline values have yet to reach their far-field values as the high stress that is developed in the

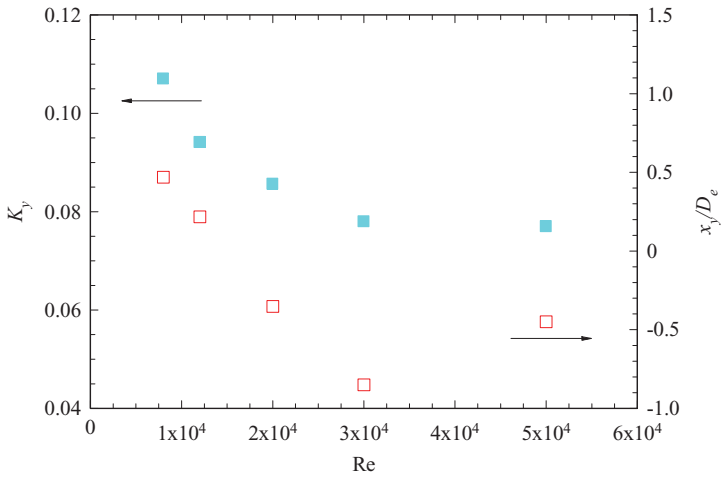

FIG. 8. Dependence of the spreading rate (K_Y) and virtual origin (x_R/D_e) on Re_d.

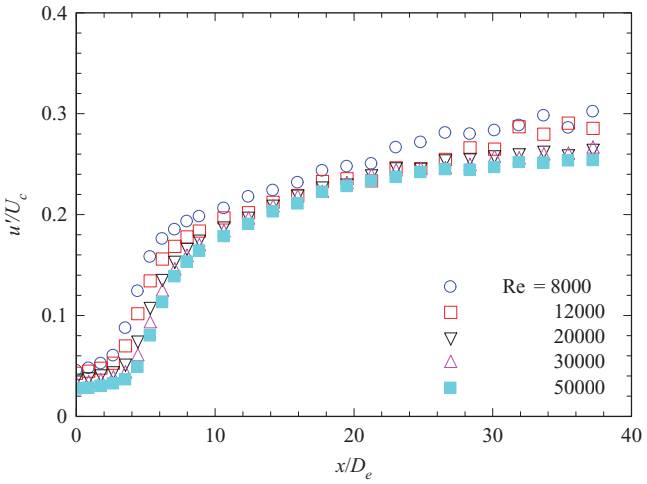

FIG. 9. Normalized streamwise RMS velocity u'/U_c along the centreline.

near field shear layers has not yet diffused to the centreline. Despite this, it appears once again that we can conclude that the critical Reynolds number is $\mathrm{Re}_{\mathrm{cr}} = 30\,000$ above which the asymptotic far-field value of K_u is independent of Re.

Figure 11 presents the lateral distributions of turbulent intensity (u'/U_c) at selected downstream positions for all Reynolds numbers considered; the y-coordinate is normalized with the half-width $Y_{1/2}$. Obviously, the turbulence intensities in the shear layer are larger than those along the centreline. In the far field, the flow develops toward equilibrium where the maximum value of u'/U_c across the jet has not reached the centreline. For each Reynolds number, the profiles of u'/U_c at different downstream positions (x/D_e) gradually converge to a self-similar profile. For instance, the self-similarity is attained at $x/D_e > 25$ for $\mathrm{Re}_d = 5 \times 10^4$ and at $x/D_e > 35$ for $\mathrm{Re}_d = 8 \times 10^3$. Compared with lateral distributions of the mean velocity, see Fig. 6, the profiles of turbulence intensity indicates that further development is required to reach self-similarity.

Figures 12 and 13 provide the centreline evolution of skewness and flatness factors of the longitudinal velocity fluctuations, S [$\equiv\langle u^3\rangle/(\langle u^2\rangle)^{3/2}$], F [$\equiv\langle u^4\rangle/(\langle u^2\rangle)^2$] for $\mathrm{Re} = 8 \times 10^3 \sim 5 \times 10^4$. These provide some measure of departure from a Gaussian probability density function (PDF) of u.

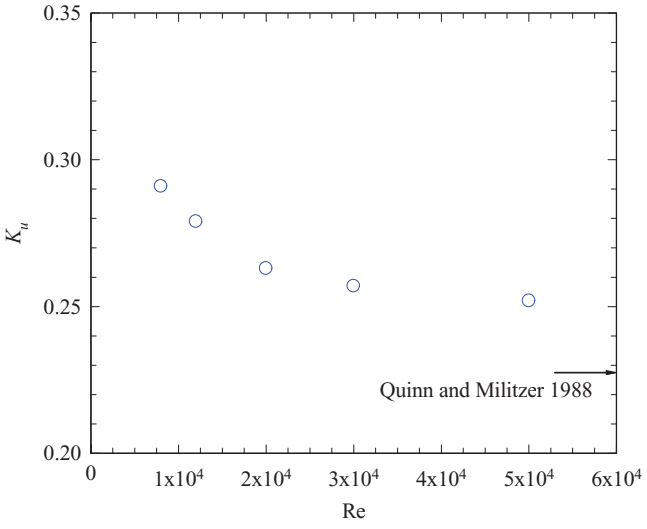

FIG. 10. Re dependence of the asymptotic value of turbulence intensity.

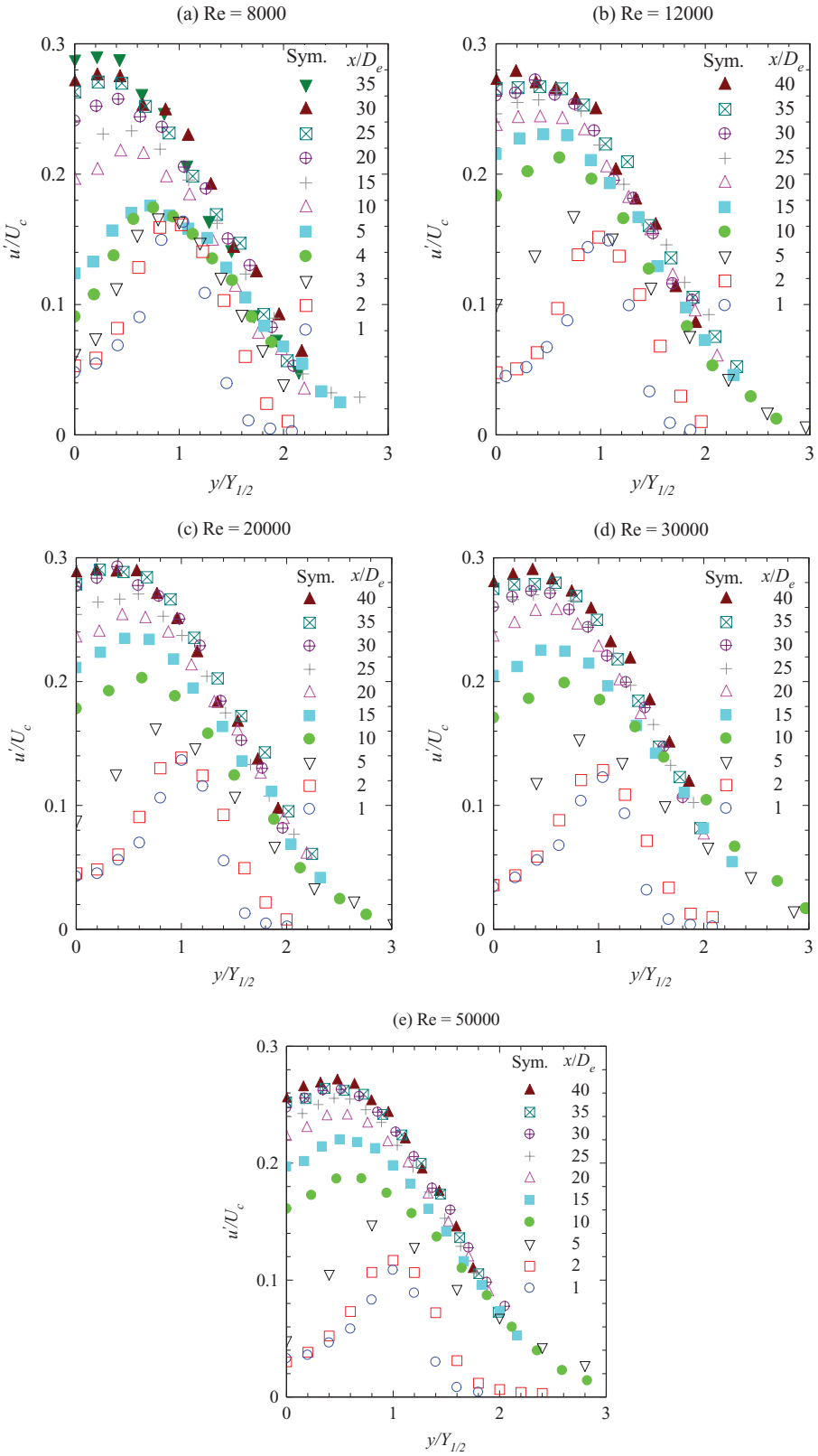

FIG. 11. Lateral distributions of u'/U_c for (a) Re = 8000, (b) = 12 000, (c) Re = 20 000; (d) Re = 30 000, (e) Re = 50 000.

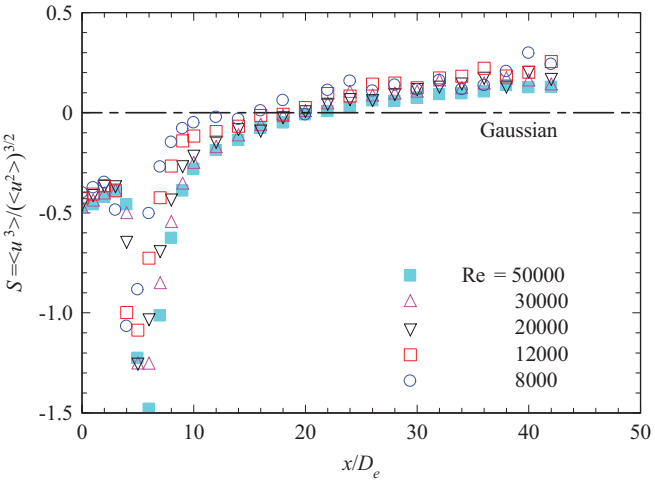

FIG. 12. Streamwise evolution of skewness for Re = 8000–50 000.

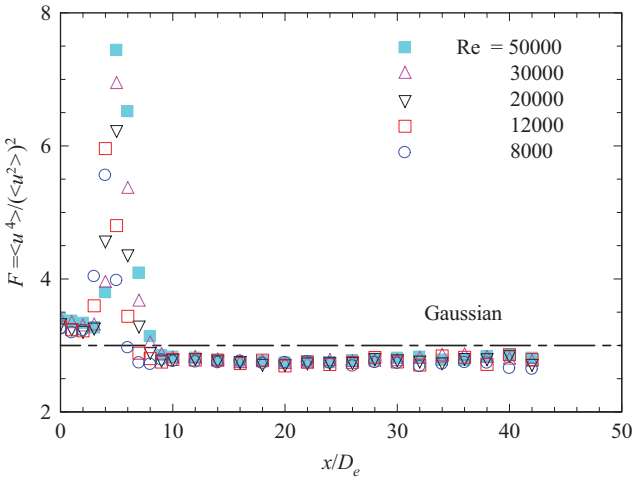

FIG. 13. Streamwise evolution of flatness for Re = 8000–50 000.

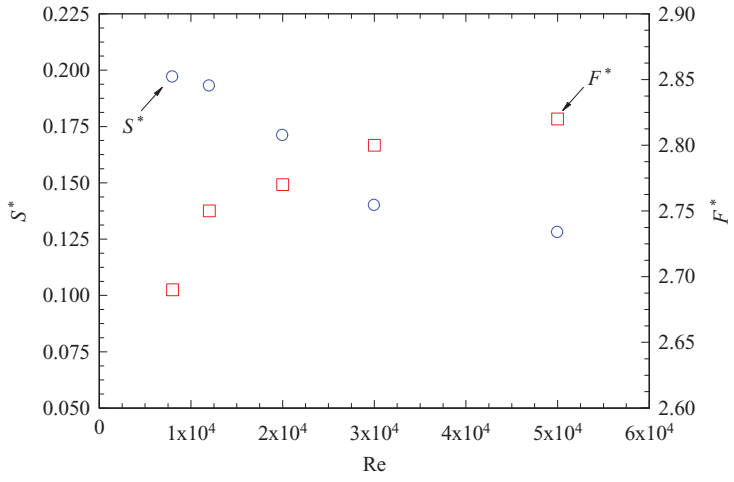

FIG. 14. Dependence of asymptotic value of $S^*$and F^*.

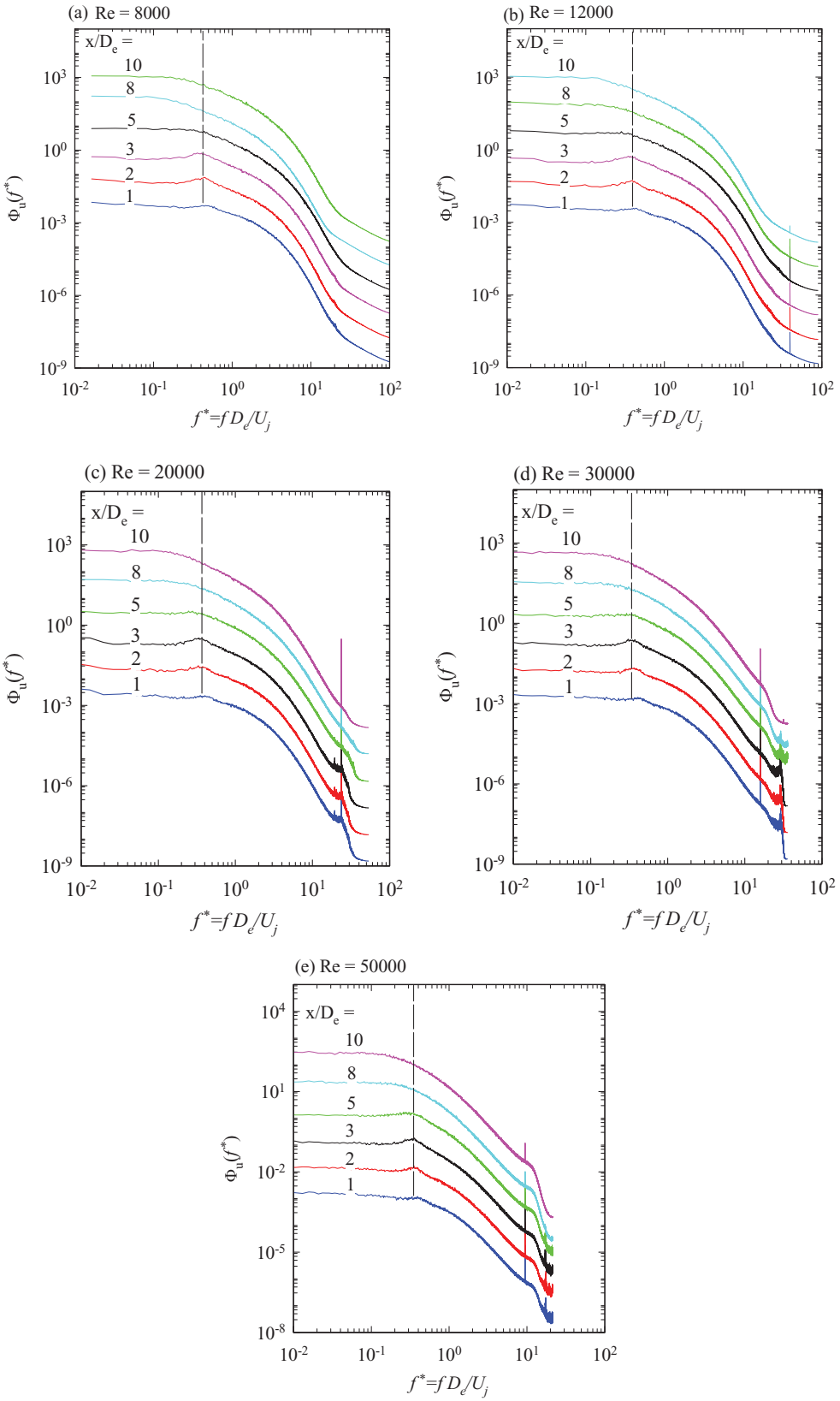

FIG. 15. Centreline spectra Φ_u of velocity fluctuation u between $x/D_e = 1$ and $x/D_e = 10$ for (a) Re = 8000, (b) Re = 12 000, (c) Re = 20 000, (d) Re = 30 000, (e) Re = 50 000.

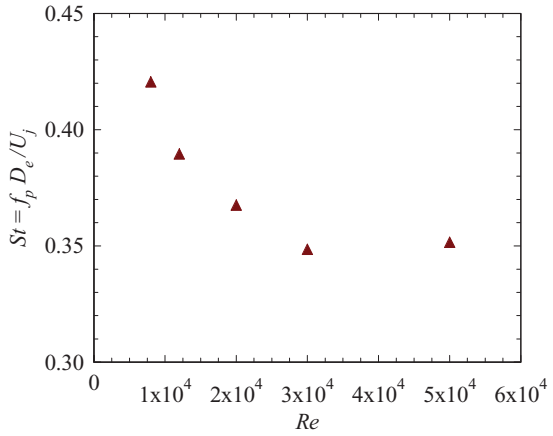

FIG. 16. Dependence of the Strouhal number $\mathrm{St} = f_p D_e/U_j$ on Re. Note that the values of the St are those of f^* that correspond to peaks of Φ_u between $x/D_e = 2$ and $x/D_e = 5$ as indicated in Fig. 14 by the dashed lines.

Both S and F were estimated from a large data set to achieve convergence of the PDF. During measurements a voltage offset was applied to the analog-to-digital range of the A/D board to ensure that neither factors were truncated due to clipping of the tails of the PDFs.

Both factors vary dramatically in the near-field region ($x/D_e < 20$) presumably due to the dominance of the large-scale coherent motions in the near-field region; see Grinstein[11] and Grinstein *et al.*[26] Farther downstream from the exit, both S and F become highly non-Gaussian, and display local maxima in the vicinity of $\mathrm{x/D_e} \sim 6$ and then recover to their asymptotic values in the far-field region ($x/D_e \geq 30$). In general, as Re is increased, the near-field maxima increase in magnitude and their x-locations shift slightly downstream. More coherent motions in the shear layers are evidenced by less random fluctuations, i.e., by more departures of the PDF from the Gaussian distribution and thus of S and F from their Gaussian values of 0 and 3, respectively. In addition, S and F approach their respective asymptotic values, $S^*$and F^* at $x/D_e \geq 30$ for all values of Re. Here, $S^*$and F^* are obtained based on the averaged value of S and F over the region $30 \leq x/D_e \leq 40$. However, both $S^*$and F^* exhibit a consistent, albeit weak, dependence on Re. Overall, as Re is increased, S^* decrease, while F^* increase (see Fig. 14); namely, the randomness of the jet, as expected, increases with increasing Re.

Figure 15 presents the centreline evolution of one-dimensional spectrum of the fluctuating velocity, Φ_u, from $x/D_e = 1$ to $x/D_e = 10$, where Φ_u is defined by $\langle u^2 \rangle = \int_0^\infty \Phi_u df$ and f denotes the frequency. The normalized frequency is defined as $f^* = fY_{1/2}/U_c$. The vertical dashed lines in the figure indicate the broad peaks in Φ_u at $x/D_e = 2{\sim}5$. Figure 16 demonstrates that very close to the nozzle at $x/D_e < 1$ no fundamental peaks can be identified in the range of $0.3 \leq f^* \leq 0.5$. In the current experiment, data were not taken off the centreline that would enable jet shear layer or preferred instability modes to be identified. Farther downstream at $x/D_e \geq 2$, such peaks, albeit weak, are present, which suggests that vortices do exist within the shear layers and their presence is detected on the centreline. The coherent structures in the shear layer probably occur weakly and infrequently because of the thick boundary layer in the exit plane, see Grinstein *et al.*[11] The gradient of the mean velocity in the shear layer is also probably not high enough to produce large-scale coherent structures. With increased distance downstream, the spectral peaks dissipate so that there no peaks in Φ_u are detected in the low frequency region. The spikes in the spectra in Figs. 15(b)–15(e) at the upper end of the frequency noise range are due to electronic (including shot, flicker, burst, etc.) noise.

Figure 16 presents the Re dependence of the Strouhal number St [$\equiv f_p D_e/U_j$] that correspond to the vertical dashed lines associated with f^* in Fig. 15. It appears that an increase in the Reynolds number from Re = 8000 to Re = 30 000 causes St to decrease, which implies some dependence on Re. Figure 16 also indicates that St is nearly independent of Re when Re ≥ 30 000.

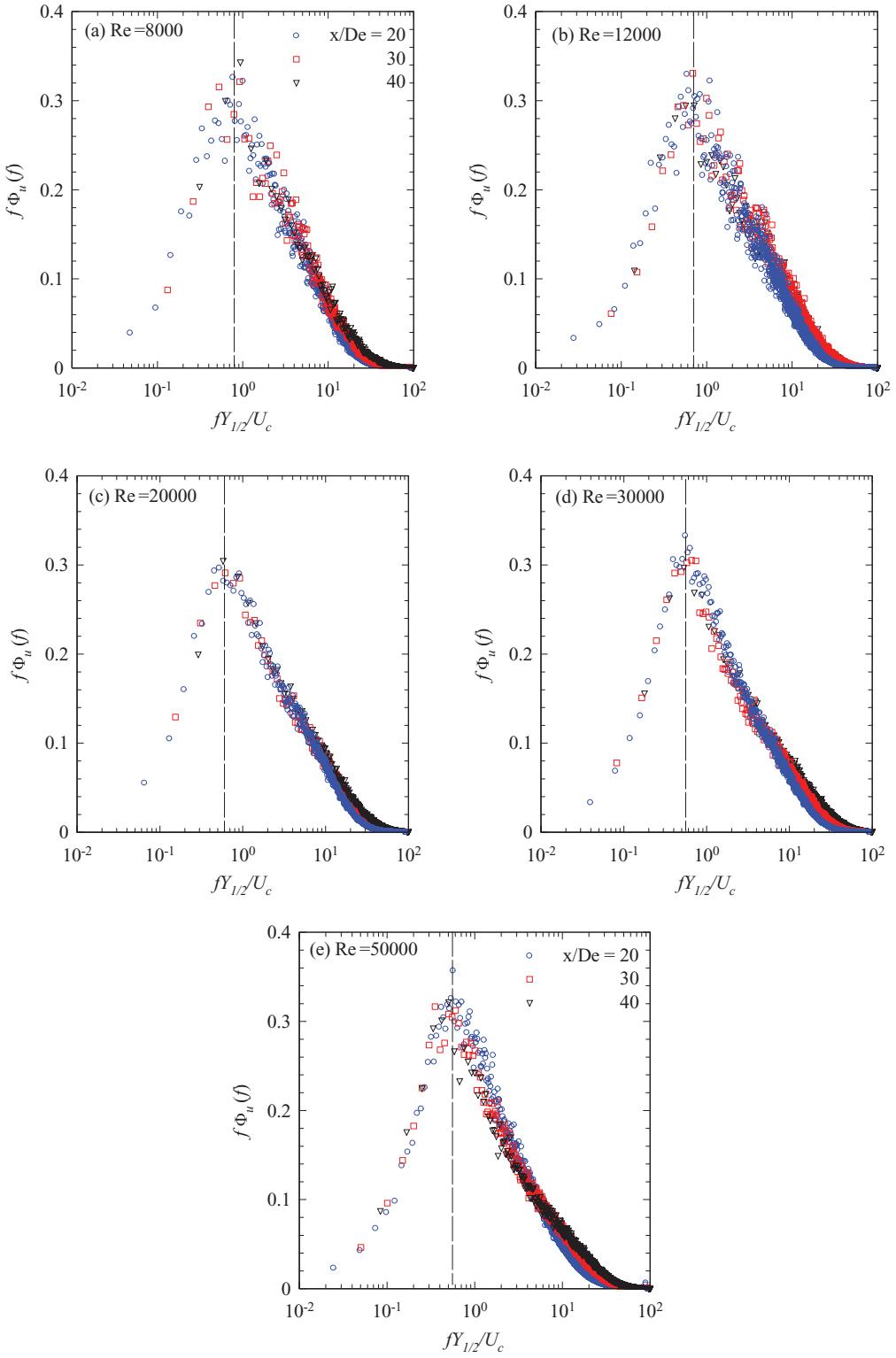

FIG. 17. Evolution of the centreline Φ_u obtained at x/D_e = 20, 30 and 40 in the form of fΦ_u vs log ($fY_{1/2}/U_c$) for (a) Re = 8000, (b) Re = 12 000, (c) Re = 20 000, (d) Re = 30 000, (e) Re = 50 000.

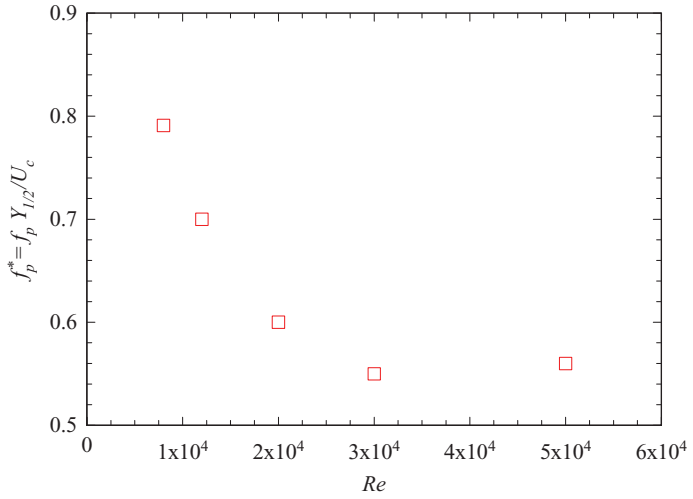

FIG. 18. Dependence of $f^*_p = f_p Y_{1/2}/U_c$ on Re.

Now, the far-field u-spectra, Φ_u, and their centreline evolution are considered for different Reynolds numbers. Figures 17(a)–17(e) present the far-field data of Φ_u, respectively, for Re = 8000–50 000, obtained at x/D_e = 20, 30, and 40 on the centreline, in the form of $f\,\Phi_u$ vs log ($f\,Y_{1/2}/U_c$) so as to identify the frequency (subscript "p") corresponding to the peak in Φ_u due to the presence of the far-field coherent structures and their quasi-periodic passage. The dimensionless frequency $f^*_p = f_p Y_{1/2}/U_c$ versus Re is presented using Fig. 18. Similar to the exit Strouhal number St reported in Fig. 16, f^*_p decreases fairly significantly (by about 30%) as Re increases from 8000 to 30 000 but changes little for Re $\geq$ 30 000. It is evident that the spectral peak of the turbulent kinetic energy is centred around $f^*_p = f_p Y_{1/2}/C_u \approx 0.5\sim0.8$ (depending on Re).

The centreline one-dimensional spectra of the fluctuating velocity (Φ_u) for x/De = 30 are presented in Fig. 19 for the five values of Re considered here. The solid and dashed lines correspond to $\sim f^{-3/2}$ and $\sim f^{-5/3}$, respectively. It appears that all these spectra exhibit a power-law region, i.e., $\Phi_u \propto f^{-m}$, over a certain range of f; clearly, as expected, the range over which f spans, widens as Re increases. Here, the frequency can be transferred to the streamwise component of the wavenumber (k_1) as $k_1 = 2\pi f/U_c$. Theoretically, $\Phi_u(k_1) = C\varepsilon^{2/3}k_1^{-5/3}$ and this applies, according to Kolmogorov, at "sufficiently large Reynolds number." Sreenivasan[44] introduced a modification

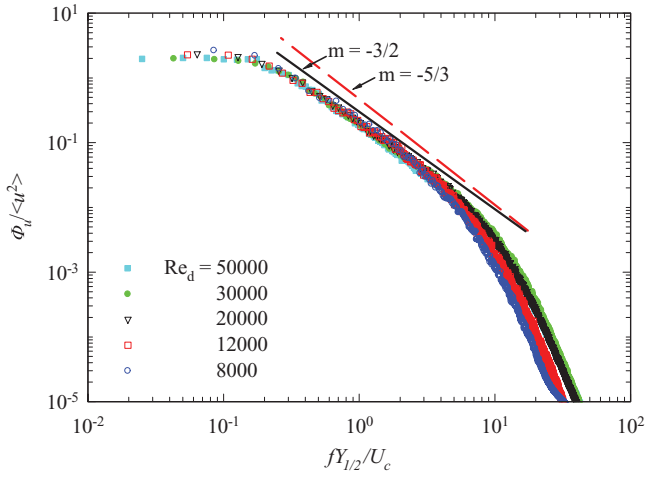

FIG. 19. Reynolds number dependent spectra of the centreline u measured at x/D_e = 30.

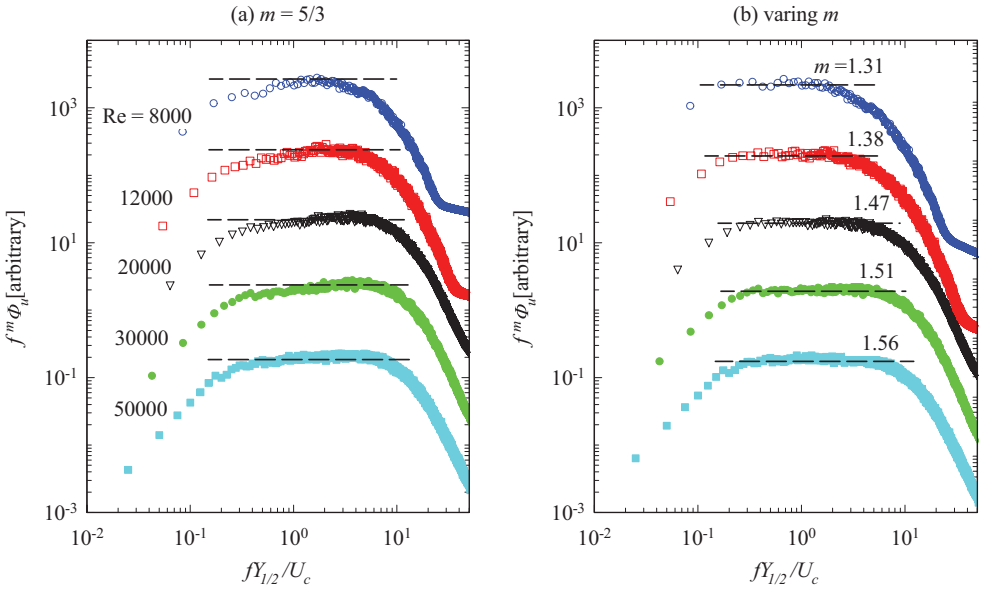

FIG. 20. Compensated velocity spectra $f^m\Phi_u$ of the centreline u measured at $x/D_e = 30$ for (a) $m = 5/3$, and (b) $m = 1.31$–1.56.

to the one-dimensional spectra, $\Phi_u(k_1) = C\varepsilon^{2/3}k_1^{-5/3}(k_1\eta)^{5/3-n1}$ and for the case of grid generated wind tunnel turbulence data, Mydlarski and Warhaft[45] noted the dependence of the k_1-exponent on the Taylor Reynolds number, R_λ, that is,

$$n_1 = (5/3)(1 - 3.15R_\lambda^{-2/3}). \tag{8}$$

Here, n_1 is identical to the exponent m, i.e., $n_1 = m$. Moreover, they noted the dependence of C on R_λ too. Gamard and George[46] noted $E(k) = Ck^{-5/3+\mu}$, where μ and C are Reynolds number dependent. Gamard and George[46] were able to demonstrate that a near-asymptotic analysis was able to capture the effects found by Mydlarski and Warhaft.[45]

Figure 20 presents the compensated spectra for the jet on the centreline at $x/D_e = 30$ for the Reynolds numbers considered. The power-law exponent (m) is not 5/3 for the current experiment, rather $m = 1.31 \sim 1.56$. That is, the exponent increases slightly with Re. Interestingly, a further

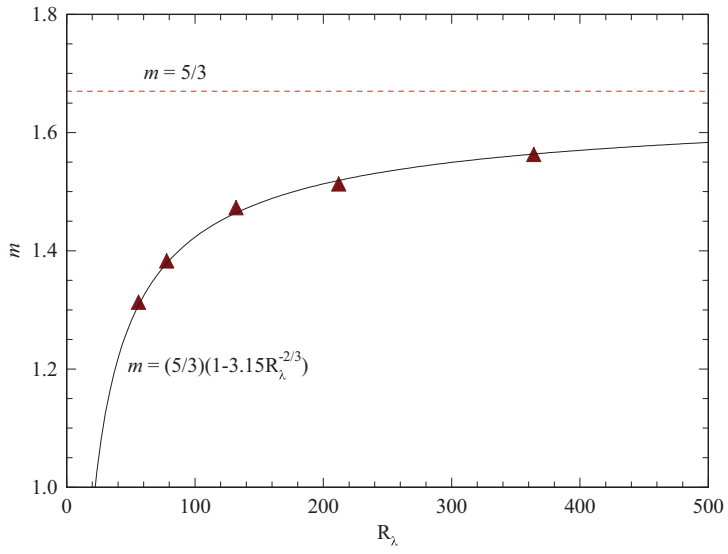

FIG. 21. The R_λ dependence of the power-law exponent of Φ_u, all for $x/D_e = 30$.

check using Fig. 21 reveals that the m-R_λ relationship for the present square jet follows that obtained by Mydlarski and Warhaft[45] for grid generated turbulence, i.e., Eq. (8). Given that the two flows are totally different, this relation may be generic for any turbulent flow where the turbulence is not intermittent. In other words, the power-law exponent, if present, of the frequency spectrum of u from any flows should depend on R_λ in the quantitative form of $m = (5/3)(1-3.15R_\lambda{}^{-2/3})$.

IV. CONCLUSION AND RECOMMENDATION FOR FURTHER WORK

The present study performed hot-wire measurements at the exit Reynolds number $Re = 8 \times 10^3 \sim 5 \times 10^4$ to examine the Re dependence of the downstream development of the turbulent jet from a long square duct. Within this Re range, significant dependences were found in the mean velocity decay rate and half-width, and in the evolution of turbulent intensity and skewness and flatness factors of the fluctuating velocity. More specifically, the main findings of the influences of Re over the range of the present investigation are summarized as follows:

(1) For $Re \leq 30\,000$, the far-field asymptotic rates of the mean velocity decay and spread, the asymptotic value of the streamwise turbulent intensity, as well as the near-field and far-field Strouhal numbers, all decrease monotonically as Re increases. However, when $Re > 30\,000$, all the above asymptotic values do not change appreciably with Re. It follows that the critical Reynolds number beyond which no further changes in jet behavior should occur at $Re_{cr} \sim 30\,000$.
(2) As Re is increased, the asymptotic value of the u skewness decreases while the asymptotic value of the flatness increases. That is, the far-field randomness of the jet increases with increasing Re.
(3) The power-law exponent (m) of the u spectrum on the jet centreline follows the relation $m = (5/3)(1-3.15R_\lambda{}^{-2/3})$ obtained by Mydlarski and Warhaft[45] for the grid generated turbulence. This finding suggests that the m-R_λ correlation of Mydlarski and Warhaft[45] may apply to other turbulent flows removed from walls.

The above dependence on the Reynolds number for $Re < 30\,000$ are believed to reflect changes in the flow conditions at the nozzle exit plane and thus changes in the downstream underlying (large-scale) flow structures. For $Re \geq 30\,000$, all the changes appear to become insignificant. Nevertheless, this critical Reynolds number is much higher than that ($\approx 10\,000$) found, e.g., Ref. 3 for round jets from a smooth contracting nozzle, where the initial flow is laminar-like with a much lower overall turbulence intensity ($<1\%$ in general) than those of the present square jets ($>5\%$). Why does such a great difference take place in the two turbulent jets? Is it because a higher value of the exit turbulence intensity and other different initial parameters in the square jet from a long pipe delay the occurrence of turbulence mixing transition (if any) proposed by Dimotakis[3] or widen the transition band? It is recommended that further work be done to confirm these suppositions.

ACKNOWLEDGMENTS

M.X. gratefully acknowledges the support of Graduate School of Peking University for his visit to Queen's University. J.M. acknowledges the support of National Science Foundation of China (NSFC) (Grant Nos. 10921202 and 11072005). A.P. acknowledges the support of the Natural Sciences and Engineering Research Council of Canada.

[1] H. Fellouah, C. G. Ball, and A. Pollard, "Reynolds number effects within the development region of a turbulent round free jet," Int. J. Heat Mass Transfer **52**(17–18), 3943–3954 (2009).
[2] H. Fellouah and A. Pollard, "The velocity spectra and turbulence length scale distributions in the near to intermediate regions of a round free turbulent jet," Phys. Fluids **21**(11), 115101 (2009).
[3] P. E. Dimotakis, "The mixing transition in turbulent flows," J. Fluid Mech. **409**(1), 69–98 (2000).
[4] A. Hussain, "Coherent structures and turbulence," J. Fluid Mech. **173**, 303–356 (1986).
[5] W. George, "The self-preservation of turbulent flows and its relation to initial conditions and coherent structures," in *Recent Advances in Turbulence*, edited by R. E. A. Arndt and W. K. George (Hemisphere, New York, 1989).

[6] G. Xu and R. A. Antonia, "Effect of different initial conditions on a turbulent round free jet," Exp. Fluids **33**(5), 677–683 (2002).
[7] M. Uddin and A. Pollard, "Self-similarity of coflowing jets: The virtual origin," Phys. Fluids **19**(6), 068103 (2007).
[8] C. Ball, H. Fellouah, and A. Pollard, "The flow field in turbulent round free jets," Prog. Aerosp. Sci. **50**, 1–26 (2012).
[9] S. R. Gollahalli, T. Khanna, and N. Prabhu, "Diffusion flames of gas jets issued from circular and elliptic nozzles," Combust. Sci. Technol. **86**(1–6), 267–288 (1992).
[10] F. F. Grinstein, "Self-induced vortex ring dynamics in subsonic rectangular jets," Phys. Fluids **7**(10), 2519–2521 (1995).
[11] F. Grinstein, E. Gutmark, and T. Parr, "Near field dynamics of subsonic free square jets: A computational and experimental study," Phys. Fluids **7**(6), 1483–1497 (1995).
[12] E. Gutmark and F. Grinstein, "Flow control with noncircular jets," Annu. Rev. Fluid Mech. **31**(1), 239–272 (1999).
[13] E. Gutmark *et al.*, "Noncircular jets in combustion systems," Exp. Fluids **7**(4), 248–258 (1989).
[14] C. Ho and E. Gutmark, "Vortex induction and mass entrainment in a small-aspect-ratio elliptic jet," J. Fluid Mech. **179**, 383–405 (1987).
[15] H. Husain and A. Hussain, "Controlled excitation of elliptic jets," Phys. Fluids **26**, 2763 (1983).
[16] F. Hussain and H. Husain, "Elliptic jets. Part 1. Characteristics of unexcited and excited jets," J. Fluid Mech. **208**, 257–320 (1989).
[17] J. Mi, G. J. Nathan, and R. E. Luxton, "Centreline mixing characteristics of jets from nine differently shaped nozzles," Exp. Fluids **28**(1), 93–94 (2000).
[18] J. Mi *et al.*, "PIV measurements of a turbulent jet issuing from round sharp-edged plate," Exp. Fluids **42**(4), 625–637 (2007).
[19] R. Miller, C. Madnia, and P. Givi, "Numerical simulation of non-circular jets," Comput. Fluids **24**(1), 1–25 (1995).
[20] W. Quinn, "Development of a large-aspect-ratio rectangular turbulent free jet," AIAA J. **32**(3), 547–554 (1994).
[21] H. Yu and S. S. Girimaji, "Near-field turbulent simulations of rectangular jets using lattice Boltzmann method," Phys. Fluids **17**, 125106 (2005).
[22] W. Quinn, "Measurements in the near flow field of an isosceles triangular turbulent free jet," Exp. Fluids **39**(1), 111–126 (2005).
[23] K. Schadow *et al.*, "Selective control of flow coherence in triangular jets," Exp. Fluids **6**(2), 129–135 (2004).
[24] K. B. M. Q. Zaman, "Axis switching and spreading of an asymmetric jet: The role of coherent structure dynamics," J. Fluid Mech. **316**(1), 1–27 (1996).
[25] K. Zaman, "Spreading characteristics of compressible jets from nozzles of various geometries," J. Fluid Mech. **383**, 197–228 (1999).
[26] F. Grinstein and C. DeVore, "Dynamics of coherent structures and transition to turbulence in free square jets," Phys. Fluids **8**(5), 1237–1251 (1996).
[27] D. Liepmann and M. Gharib, "The role of streamwise vorticity in the near-field entrainment of round jets," J. Fluid Mech. **245**, 643–668 (1992).
[28] J. Citriniti and W. George, "Reconstruction of the global velocity field in the axisymmetric mixing layer utilizing the proper orthogonal decomposition," J. Fluid Mech. **418**, 137–166 (2000).
[29] S. McIlwain and A. Pollard, "Large eddy simulation of the effects of mild swirl on the near field of a round free jet," Phys. Fluids **14**, 653 (2002).
[30] A. Pinelli *et al.*, "Reynolds number dependence of mean flow structure in square duct turbulence," J. Fluid Mech. **644**, 107–122 (2010).
[31] E. Brundrett and W. Baines, "The production and diffusion of vorticity in duct flow," J. Fluid Mech. **19**(03), 375–394 (1964).
[32] T. Kajishima and Y. Miyake, "A discussion on eddy viscosity models on the basis of the large eddy simulation of turbulent flow in a square duct," Comput. Fluids **21**, 151–161 (1992).
[33] A. Melling and J. Whitelaw, "Turbulent flow in a rectangular duct," J. Fluid Mech. **78**(part 2), 289–315 (1976).
[34] B. Launder and W. Ying, "Secondary flows in ducts of square cross-section," J. Fluid Mech. **54**(part 2), 289–295 (1972).
[35] F. Gessner and A. Emery, "The numerical prediction of developing turbulent flow in rectangular ducts," J. Fluids Eng. **103**, 445 (1981).
[36] J. Mi and R. A. Antonia, "Effect of large-scale intermittency and mean shear on scaling-range exponents in a turbulent jet," Phys. Rev. E **64**(2), 026302 (2001).
[37] J. Mi and R. A. Antonia, "Vorticity characteristics of the turbulent intermediate wake," Exp. Fluids **20**(5), 383–392 (1996).
[38] J. Mi, R. C. Deo, and G. J. Nathan, "Fast-convergent iterative scheme for filtering velocity signals and finding Kolmogorov scales," Phys. Rev. E **71**(6), 066304 (2005).
[39] J. Mi, M. Xu, and C. Du, "Digital filter for hot-wire measurements of small-scale turbulence properties," Meas. Sci. Technol. **22**, 125401 (2011).
[40] S. Pope, *Turbulent Flows*, 1st ed. (Cambridge University Press, 2000).
[41] R. C. Deo, J. Mi, and G. J. Nathan, "The influence of Reynolds number on a plane jet," Phys. Fluids **20**(7), 075108 (2008).
[42] H. Yu, L. S. Luo, and S. S. Girimaji, "LES of turbulent square jet flow using an MRT lattice Boltzmann model," Comput. Fluids **35**(8–9), 957–965 (2006).
[43] W. Quinn and J. Militzer, "Experimental and numerical study of a turbulent free square jet," Phys. Fluids **31**, 1017 (1988).
[44] K. Sreenivasan, *On Local Isotropy of Passive Scalars in Turbulent Shear Flows* (The Royal Society, 1991).
[45] L. Mydlarski and Z. Warhaft, "On the onset of high-Reynolds-number grid-generated wind tunnel turbulence," J. Fluid Mech. **320**(1), 331–368 (1996).
[46] S. Gamard and W. K. George, "Reynolds number dependence of energy spectra in the overlap region of isotropic turbulence," Flow, Turbul. Combust. **63**(1), 443–477 (2000).